Interpretable artificial intelligence framework for COVID-19 screening on chest X-rays

NIKOS TSIKNAKIS[1], ELEFTHERIOS TRIVIZAKIS[1,2], EVANGELIA E. VASSALOU[3,4],

GEORGIOS Z. PAPADAKIS[1,2], DEMETRIOS A. SPANDIDOS[5], ARISTIDIS TSATSAKIS[6],

JOSE SÁNCHEZ-GARCÍA[7], RAFAEL LÓPEZ-GONZÁLEZ[7,8], NIKOLAOS PAPANIKOLAOU[1,9],

APOSTOLOS H. KARANTANAS[1-3] and KOSTAS MARIAS[1,10]

[1]Computational Biomedicine Laboratory (CBML), Foundation for Research and Technology Hellas (FORTH),
70013 Heraklion; [2]Department of Radiology, Medical School, University of Crete, 71003 Heraklion; [3]Department of
Medical Imaging, University Hospital of Heraklion, 71110 Heraklion; [4]Department of Radiology, District Hospital,
72300 Lasithi; [5]Laboratory of Clinical Virology; [6]Department of Forensic Sciences and Toxicology,
Medical School, University of Crete, 71003 Heraklion; [7]QUIBIM S.L., 46021 Valencia; [8]Universidad de Valencia,
46010 Valencia, Spain; [9]Computational Clinical Imaging Group, Centre for the Unknown,
Champalimaud Foundation, 1400-038 Lisbon, Portugal; [10]Department of Electrical and
Computer Engineering, Hellenic Mediterranean University, 71410 Heraklion, Greece

Abstract. COVID-19 has led to an unprecedented healthcare crisis with millions of infected people across the globe often pushing infrastructures, healthcare workers and entire economies beyond their limits. The scarcity of testing kits, even in developed countries, has led to extensive research efforts towards alternative solutions with high sensitivity. Chest radiological imaging paired with artificial intelligence (AI) can offer significant advantages in diagnosis of novel coronavirus infected patients. To this end, transfer learning techniques are used for overcoming the limitations emanating from the lack of relevant big datasets, enabling specialized models to converge on limited data, as in the case of X-rays of COVID-19 patients. In this study, we present an interpretable AI framework assessed by expert radiologists on the basis on how well the attention maps focus on the diagnostically-relevant image regions. The proposed transfer learning methodology achieves an overall area under the curve of 1 for a binary classification problem across a 5-fold training/testing dataset.

Correspondence to: Dr Kostas Marias, Computational Biomedicine Laboratory (CBML), Foundation for Research and Technology Hellas (FORTH), 100 N. Plastira Street, Vassilika Vouton, 70013 Heraklion, Greece
E-mail: kmarias@ics.forth.gr

Introduction

At the dawn of 2019 the World Health Organization (WHO) was notified by the Chinese authorities on novel coronavirus (2019-nCoV) causing severe respiratory illness emerging from Hubei Providence of China and particularly linked to the seafood market of Wuhan city (1). The clinical characteristics of the disease are non-specific and comprise fever, cough, fatigue and shortness of breath in the majority of cases (2). Other factors that contribute to the lethality and severity of the cases include obesity (3), chronic cardiovascular diseases (4) and smoking habits (5). Many attempts for an effective vaccine are currently under development (6) and traditional antiviral antibacterial and anti-inflammatory agents such as zinc (7) has been used to reduce the risk of co-infections. Imaging investigation, in the context of chest X-rays or computed tomography (CT) has a vital role in disease management. Bilateral airspace opacities showing a peripheral and lower-zone predominance represent the most frequent findings on both modalities (1,8-10). Additionally, it has been reported that chest X-ray screening for asymptomatic carriers of COVID-19 may serve as a viable substitute for the available reverse transcription-quantitative polymerase chain reaction (RT-qPCR) tests (11,12). The high infection rate of COVID-19 caused, in a short period of time, an unprecedented burden on the healthcare systems, pushing intensive care units (ICU) treating multimorbid or other high-risk patients to the limits. Therefore, as recently reported, given the shortages and delays in PCR tests, chest X-rays have become one of the fastest and most affordable ways for doctors to triage patients (13). As a result, faced with staff shortages and overwhelming patient loads, a growing number of hospitals are turning to automated tools to support them manage the pandemic. In such a context artificial intelligence (AI) COVID-19 classification systems

based on chest X-rays represent a cost-beneficial solution for the early detection/diagnosis of infection and timely risk stratifications of patients.

The recent COVID-19 pandemic initiated an abundance of unpublished preprints available on open databases claiming accuracy (ACC) scores up to 99% (14-20) for COVID-19 screening on chest X-rays. These deep learning models incorporate a variety of architectures such as Generative Adversarial Networks (GANs) for data augmentation, capsule networks and transfer learning techniques. Most notably, SqueezeNet was used with Bayesian hyperparameter optimization achieving an ACC of 98.3% (21). Transfer learning techniques are crucial for deep learning model convergence on limited data, since there is a scarcity of a large and widely available COVID-19 imaging repository. Many transfer learning models have been tested on small X-ray datasets with ACC up to 98.75% for binary (COVID and normal) and among three classes, with pneumonia being the third, up to 93.48% (22). Moreover, GANs have been used jointly with transfer learning (23) to further augment the limited COVID X-ray pool improving the prediction performance with an ACC of 99.9%. Additionally, CT semantic features related to COVID-19 were similarly observed (9) and a significant detection sensitivity (SEN) of the disease of 88% was reported (10).

A self-supervised encoder deep learning architecture was deployed on raw CT slices achieving an area under the curve (AUC) of 94% (24). This impressive performance was challenged by the poor results of Grad-CAM attention maps mainly denoting regions with high contrast but irrelevant to the lung parenchyma. This effect can be attributed to the lack of a proper preprocessing protocol including image resolution normalization and lung segmentation, as well as limitations in the proposed interpretable framework. Zhao *et al* (25) composed a COVID-19 CT dataset with selected lesion slices achieving an AUC of 82.9%. On the other hand, deep models trained with similar data but evaluated on external testing sets reported AUC up to 90% (26,27). Current scientific evidence suggests that AI can provide the necessary tools for a fast, accessible and accurate screening process based on imaging data such as X-rays or CT examinations, although a robust interpretability framework, which is also evaluated by clinical experts with years of experience, remains an unmet need.

This study proposes a deep learning-based COVID-19 classification system based on X-rays. The main novelty of our proposed model lies in the classification of COVID-19 against common pneumonia cases and not normal (healthy) ones. The discrimination between COVID-19 and other, especially those of viral origin, pneumonias is intuitively more complex given the non-specific clinical signs and symptoms (2). Another advantage of our proposed pipeline relies on the evaluation of the attention maps that are created for each prediction, which represents a basic interpretability step aiming to increase trust in the final decision. The proposed method outperforms the state of the art with respect to the binary and quaternary classification tasks of Pneumonia vs COVID-19, achieving an average AUC=1, ACC=100%, SEN=99%, specificity (SPC)=100% for the binary classification and AUC=93, ACC=76%, SEN=93%, SPC=87% for the quaternary classification, across 5 folds. The model also performs close

Table I. Dataset examined patient cohort.

Examined classes			
Normal	COVID-19	Bacteria pneumonia	Virus pneumonia
150	122	150	150

to the state of the art with respect to the ternary classification task (i.e., normal, pneumonia, COVID-19). To assess the relevance of the generated attention maps, they were rated by expert radiologists in order to evaluate whether the proposed solution could evolve into an interpretable diagnostic framework.

Materials and methods

Dataset. In this study, we used two fully anonymized chest X-ray datasets of COVID-19 cases. The first one is the publicly available dataset shared by Cohen *et al* (28), which is continually updated with new cases. It consists of chest X-ray and CT images of several syndromes, such as acute respiratory distress syndrome (ARDS), COVID-19, Middle East respiratory syndrome (MERS), pneumonia, and severe acute respiratory syndrome (SARS). The X-ray dataset was accessed on the 11th of April 2020, when it included 216 COVID-19 positive cases. For this study, 115 postero-anterior (PA) X-ray views were extracted. We have chosen only the PA view, because as it represents the most commonly used radiological investigation in the emergency department (29), it is available in the corresponding pneumonia dataset. The second COVID-19 dataset originated from the QUIBIM imagingcovid19 platform database and various public repositories, including RSNA, IEEE, RadioGyan and the British Society of Thorathic Imaging. All these sources provided data mostly from Italy, Argentina, Mexico, and India, and consist of 22 PA X-ray views of patients with determined COVID-19 pneumonia. These two datasets were subsequently combined into one set, effectively forming the final COVID-19 dataset of 137 images used in this study. In addition, we used a publicly available X-ray dataset of patients with pneumonia (30,31), since our ultimate objective was to perform a multiclass classification between normal, COVID-19 and pneumonia subjects utilizing sole X-ray data. The pneumonia dataset consisted of 5,856 X-ray images categorized into 3 classes, i.e., 1,583 normal (healthy) cases, 2,780 and 1,493 pneumonia positive cases caused by bacteria and viruses (other viruses apart from COVID-19), respectively. In order to ensure balance in sample size across datasets (Table I), we randomly selected 150 images from each class, for the purposes of our study.

Preprocessing and augmentation. The images were resized to 512 by 512 pixels, and were sample-wise normalized to zero mean and unit variance. A real-time image augmentation technique was used during training, in order to enhance the size and quality of the training dataset. Specifically, we utilized

Table II. Evaluation grading system of Attention maps.

Grades	
0	The attention map is mostly homogeneous across the entire image[a]
1	The attention map is focusing on totally irrelevant areas outside the lung[b]
2	The attention map is focusing on the lung areas but also on other extrapulmonary structures[c]
3	The attention map is focusing mostly on the lung areas[d]
4	The attention map is focusing exclusively on the lung areas[e]

[a]Purple color is dominating the image. [b]All areas (100%) of blue, green and yellow exist only outside the lungs. [c]Up to 50% of areas of blue, green and yellow are located within the lungs. [d]Almost all areas (50-99%) of blue, green and yellow exist within the lungs. [e]All areas (100%) of blue, green and yellow are located only within the lungs.
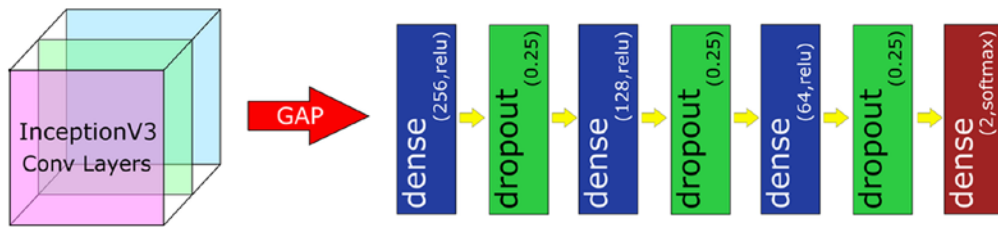

Figure 1. Proposed architecture classifiers.

the ImageDataGenerator class of Keras (https://keras.io). The augmentation options included geometrical distortions such as small rotations, shearing and zooming up to a factor of 20%.

Model architecture. Hyperparameter optimization was used to identify the highest performing pretrained model (Inception V3) for differentiating the examined COVID-19 X-rays. The proposed model's pipeline includes two main deep learning components. The first one is a convolutional neural network (CNN) backbone network without its fully connected layers, namely the Inception-V3 (32). The Inception-V3 was trained on the ImageNet database (33), which consists of approximately 14 million images divided into a thousand classes. It is worth stating that transfer learning has been successfully utilized in numerous medical imaging problems, such as diabetic retinopathy detection from fundus images (34). The second component of the model's pipeline is a standard deep neural network classifier (Fig. 1). It consists of a global average pooling (GAP) layer, 3 fully-connected layers of 256, 128 and 64 neurons, respectively, each activated by a ReLU function, and followed by a Dropout layer with 25% dropout rate. The GAP layer computes the mean value of each feature map, effectively downscaling and flattening the output of InceptionV3. A final n-neuron layer follows, which includes 2-neurons for binary classification, 3-neurons for ternary classification and 4-neurons for quaternary classification, with softmax activation function being applied.

Evaluation of transfer learning methods. The trained models were evaluated in the unseen testing sets across 5 folds. The metrics used are prediction ACC, SEN, precision (PRE), AUC score for the binary, AUC one versus rest (AUC OvR) and AUC one versus one (AUC OvO) for the multiclass classification:

$$ACC = (TP+TN) / (TP+FP+TN+FN)$$

$$SEN = TP / (TP+FN)$$

$$SPC = TN / (TN+FP)$$

$$PRE = TP / (TP+FP)$$

Interpretability. In order to enhance the model's interpretability, we applied the GradCAM (35) algorithm to visualize the importance of each pixel on the final decision. GradCAM examines the gradient information flowing from the input layer up to the last convolutional layer, for a given class label, providing a qualitative attention map for assessing the performance of the network. In particular, in order to generate the class-discriminative localization map Grad-CAM computes the gradients of the score for class c before the softmax, y^c, with respect to the last set of feature maps of the CNN A^k (i.e., the output of the last convolutional block, exactly before the FCN), i.e., $\partial y^c / \partial A^k$. To obtain the weights of the neurons importance, the new gradients are computed by the global average pooling layer over the dimensions of the image a_k^c. Finally, a linear combination of the weights and the feature maps is applied, followed by a ReLU function, to produce the heatmap. The heatmap was subsequently resized to the initial dimension of the image and overlaid on it. It should be noted that these visualizations are based on the output of the convolutional part of the network but not on the classification part. Thus, the fully connected layers of the classification network may further process these features, effectively applying a selection strategy on them, in order to predict the final outcome. As a result, caution is required when interpreting the visualizations, as they are simply indications of where the Deep Learning System is 'looking at' in order to make its decision.

Table III. Performance evaluation of the current literature and the proposed transfer learning model in terms of binary (COVID vs. pnemonia), ternary (normal, COVID, pnemonia), quaternary (normal, COVID, bacterial pneumonia, viral pneumonia) classification.[a]

Type %	ACC	SEN	SPC	AUC
Binary				
Proposed	**100±1.0**	**99±2.0**	**100±0.0**	**100±0.0**
Zhang *et al* (14)	-	up to 96	70.6	95.1
Narin *et al* (15)	98.0	96.0	**100.0**	-
Afshar *et al* (17)	98.3	80.0	98.6	-
Khalifa *et al* (19)	98.7	98.7	98.7	-
Apostolopoulos *et al* (22)	96.7	98.6	96.46	-
Chowdhury *et al* (37)	98.3	96.7	**100.0**	99.8
Ternary				
Proposed	85±7.0	94±6	92.7±7.6	96±2.0
Wang *et al* (16)	92.6	91.3	-	-
Abbas *et al* (18)	95.1	**97.9**	91.8	-
Ucar *et al* (21)	98.2	-	**99.1**	-
Apostolopoulos *et al* (22)	94.7	-	-	-
Chowdhury *et al* (37)	**98.3**	96.7	99.0	**99.0**
Quaternary				
Proposed	**76±8.0**	**93±9**	**91.8±7.6**	**93±3.0**

[a]The metrics are presented in mean ± standard deviation format, regarding the COVID-19 class for each case. The best performance is presented in bold. ACC, accuracy; SEN, sensitivity; SPC, specificity; AUC, area under the curve.

In order to validate the interpretability of the generated attention maps, we asked two experienced radiologists to rate these attention maps, based on how close they are with respect to the actual region of diagnostic interest. For each image they provided two grades, one for each hemithorax (lung). The grading scale ranged from 0 to 4. Details regarding the utilized grading scale are provided in Table II. Any difference between the grading of each expert was resolved via consensus between both experts.

Results

Model convergence. Our model was trained for 20 epochs, using the categorical cross-entropy loss function (equation 1) and Adam optimizer (36) with a batch size of 8.

$$CE = - \sum_{i}^{C} t_{iloglog\,(f(si))} \,(1)$$

where C is the total number of classes, t_i is the one-hot-encoded ground truth and $f(s_i)$ is the prediction probability for a given sample *s*.

Also, we used an exponentially decaying learning rate with an initial value of 0.001 and a decay rate of 0.96. The CNN InceptionV3 backbone's layers were 'frozen', so that only our custom classifier would be trained. The model was trained on a stratified 5-fold cross validation schema, utilizing one fold for the independent testing and the rest for training and validation purposes. The validation set was used for early-stopping during the training phase. The k-fold separation schema ensured that we can iteratively test the trained models on the whole dataset providing a clearer insight on its performance, while at the same time the training, validation and testing sets do not overlap amongst themselves on the one hand, and across all folds on the other. The validation set was randomly selected as a 10% subset of the training/validation folds, while 90% was used for training. The model was trained on a server with an AMD EPYC 7251 8-core 2.9GHz CPU, RTX 2080Ti 11GB GPU and 64GB RAM, and it was implemented on Tensorflow 2.1, utilizing the Keras module. The source code is available at the following GitHub repository (https://github.com/tsikup/COVID-19-xray-cnn).

Binary classification. We initially trained the model for detecting pneumonia and COVID-19 cases. Given that our COVID-19 dataset has a size of 137 and since our pneumonia dataset consisted of 300 cases (150 of each subclass i.e., bacteria and virus), we randomly sampled 75 images from each pneumonia subclass, so that we generated balanced datasets. As a result, the dataset for binary classification consisted of 150 pneumonia (75 of each pneumonia subclass) and 137 COVID-19 X-ray images. Table III (Binary row) provides information regarding the average performance of the models trained and tested on their respective folds. Our method consistently achieves 100% in all metrics for every fold except the third one, in which the model displayed only one false negative and no false positive results, achieving a SEN of 99%, SPC of 100%, PRE of 100%, an ACC of 100% and an AUC of 1. It is evident from these results that the model can successfully distinguish and correctly detect the two classes, i.e., pneumonia versus COVID-19. Fig. 2 illustrates the average confusion matrix across the 5 folds. The confusion matrix of each individual fold can be found in the supplementary
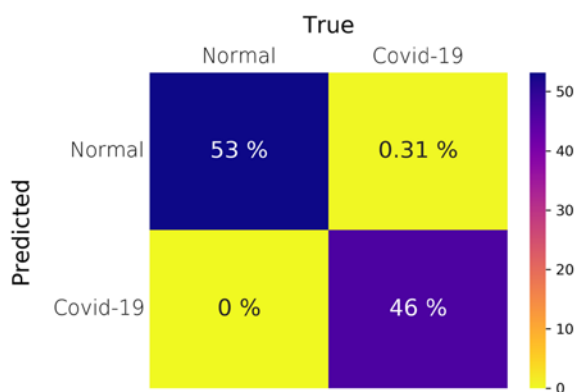
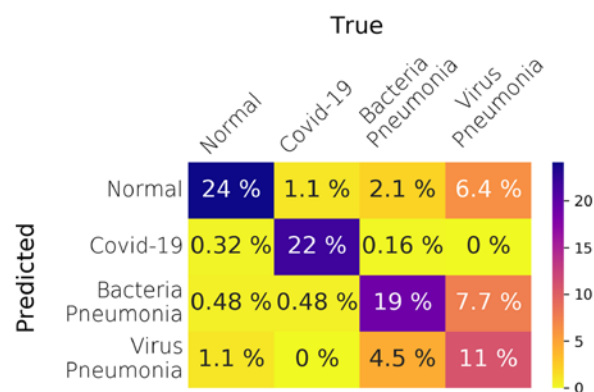Figure 2. Average confusion matrix across all folds - Binary classification.

Figure 4. Average confusion matrix across all folds - Quaternary classification.
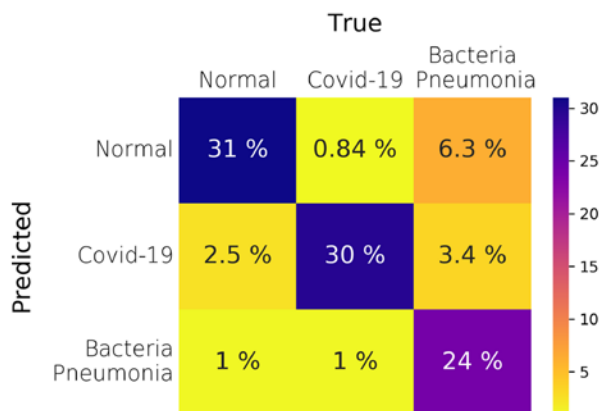

Figure 3. Average confusion matrix across all folds - Ternary classification.

document (Fig. S1). It should be noted that, although the SEN is 99% due to the one false-negative prediction, the ACC and AUC are reported as 100% and 1, respectively, due to the 2nd floating point rounding procedure of the metrics.

Ternary classification. Subsequently, we trained the model for detecting normal, pneumonia and COVID-19 cases. We also utilized the subsampled pneumonia dataset, as previously explained in the Binary classification section. Fig. 3 illustrates the average confusion matrix across the 5 folds. The proposed model performs very well in terms of the AUC metric in the One-vs-Rest testing schema, achieving a mean value of 96% across all testing folds (Table III - Ternary row). However, the mean ACC across all folds and classes is 85%, which is lower than that observed in the Binary classification task. In order to better understand the performance of the model, we present the per-class analysis across all folds in supplementary Tables SI-SIII. It becomes evident that the model performs better when it comes to predicting the COVID-19 cases instead of the Pneumonia cases, since the COVID-19 SEN has a mean value of 94% as compared to the Pneumonia one of only 72%, as reported in supplementary Tables SII and SIII. However, the false positives and the SPC values are worse for the COVID-19 class than those of the pneumonia. Thus, although the model performs well on predicting the true COVID-19 cases, it is possible that it can misclassify some normal and pneumonia cases as COVID-19 ones. Such false positives need to be eliminated, since in real deployment they could potentially lead to exposing healthy or

non-COVID-19 pneumonia patients, to COVID-19 patients risking infection expansion. As a result, the presented ternary classification requires further improvement before it can be safely used in clinical routine.

Nonetheless, the model performs quite well regarding the COVID-19 class, achieving an SPC of 92%, SEN of 94%, PRE of 86% and ACC of 92% (Table SII). As seen in the confusion matrices of each fold (Fig. S2), the COVID-19 false positives for the first fold (a) are 18, which is much higher than the other 4 folds, in which the false positives are 0 (folds 2 and 5) and 5 (folds 3 and 4). It is our view that in order to properly verify the model and explain such an inconsistency, a much larger training and testing datasets are needed.

Quaternary classification. The final experiment regards the quaternary classification between all classes of the dataset, i.e., normal, COVID-19, bacterial pneumonia and viral pneumonia cases. The overall performance of the model for the quaternary classification is worse than any of the previous tasks, with a mean ACC of 76% and an AUC of 93%. Fig. 4 illustrates the average confusion matrix across the 5 folds.

However, as shown in the per-class performance tables (Tables SIV-SVII), the model performs far better regarding the COVID-19 class with less false positives than the one in the ternary classification task, which leads to higher SPC (99%). In addition, the performance of the model regarding the normal class is approximately the same as the one in the ternary classification.

The model's performance degrades in the last two classes, i.e., bacterial and viral pneumonia cases. Especially in the viral pneumonia, the SEN of the model is far worse than any other class, reaching a mean value of 44% and a median value of 48%. By looking at the relevant confusion matrices, Fig. S3, the viral pneumonia cases are misclassified as either bacteria pneumonia or normal healthy cases. In addition, in fold 3 many bacterial pneumonia cases are misclassified as viral pneumonia. Overall, splitting the pneumonia cases in two separate subclasses, i.e., bacterial or viral, has helped the model to better predict the COVID-19 cases against all other, which is the desired task in this preliminary study.

Attention maps. In this section we report some of the exported attention maps, which visualize the convolutional part of the network as previously discussed in the Interpretability section.
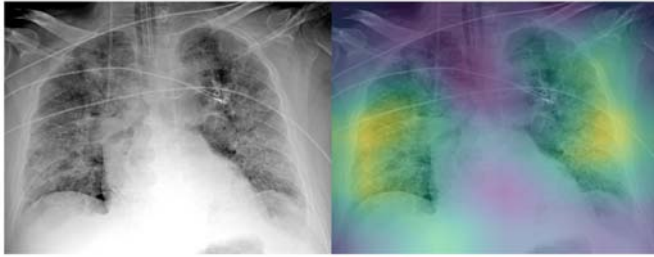
Figure 5. Attention map of patient 23 - Binary classification - True positive COVID-19 with a certainty of 100% - Evaluated as grade 2 and 3 (left and right lungs, respectively) by the experts.

Figure 8. Attention map of patient 8 - Ternary classification - False negative COVID-19 (predicted as pneumonia with a certainty of 73%) - Evaluated as grade 3 and 4 (left and right lungs, respectively) by the experts.
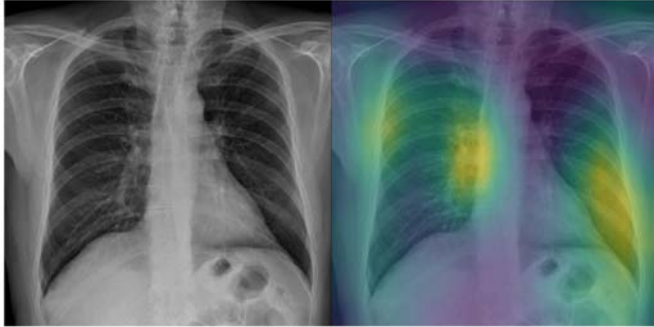

Figure 6. Attention map of patient 28 - Binary classification - True positive COVID-19 with a certainty of 100% - Evaluated as grade 3 (both left and right lungs) by the experts.

Figure 9. Attention map of patient 15 - Ternary classification - False Negative COVID-19 (predicted as pneumonia with a certainty of 53%) - Evaluated as grade 2 and 4 (left and right lungs, respectively) by the experts.

Figure 7. Attention map of patient 27 - Ternary classification - True positive COVID19 (predicted as COVID-19 with a certainty of 100%) - Evaluated as grade 0 and 4 (left and right lungs, respectively) by the experts.

Figure 10. Attention map of patient 10 - Ternary classification - False negative COVID-19 (predicted as normal with a certainty of 95%) - Evaluated as grade 2 and 2 (left and right lungs, respectively) by the experts.

Figs. 5 and 6 visualize the attention maps of two COVID-19 patients regarding the binary classification model, while Figs. 7-10 present the results for the ternary classification task. In order to accelerate the clinical acceptance of AI classification systems there is an ongoing effort to assess the interpretability potential of the proposed solutions. In our case, we hypothesize that 'attention' to diagnostically irrelevant regions in the image is an indication of randomness and reduced generalizability.

The evaluation of the attention maps from two expert radiologists is presented here. Rating was done on two randomly selected testing sets of positively COVID-19 classified images from the binary and the ternary classification tasks. The model had predicted all of the images as COVID-19 correctly for the binary classification and all but 4 for the ternary classification task. Regarding the ternary classification the model had misclassified 2 images as pneumonia and 2 as normal.
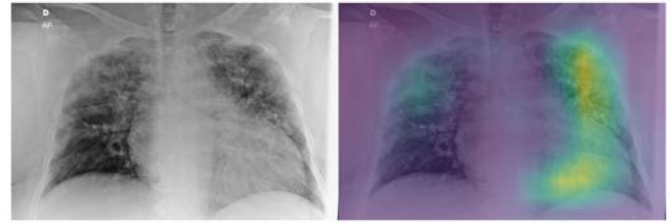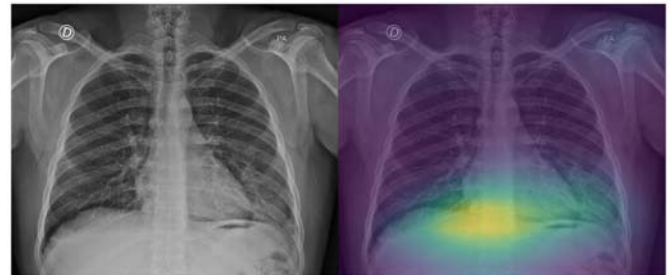
The evaluation results can be found in Tables IV and V, while Tables VI and VII report the disagreements of the experts on the first and second testing set, respectively. Regarding the binary classification testing set, the model focuses on relevant regions mostly inside the lung for half of the samples (grade 3). The fact that the model 'looks' at these regions is very promising because they may be relevant to diagnosing COVID-19. The fact that the model also focuses on other regions outside the lungs (grade 2) for the other half of samples indicates that training on a much larger dataset is needed, so that the model exhibits a more robust performance in that respect.

On the other hand, regarding the second testing set, there are a few cases that the model does not focus on a specific region of the X-ray image for predicting COVID-19 (grade 0 - e.g., patient's left lung, Fig. 7), while there are also some perfectly focused attention maps (grade 4). However, most of the gradings are reported, similarly to those in the

Table IV. Evaluation of Attention maps by 2 radiologists regarding the Binary classification.

		Grades				
	Lung	0	1	2	3	4
Expert 1	Left	0	0	16	12	0
	Right	0	0	9	18	1
Expert 2	Left	0	0	14	14	0
	Right	0	0	9	19	0
Consensus	Left	0	0	17 (60%)	11 (40%)	0
	Right	0	0	9 (32%)	19 (68%)	0

Table V. Evaluation of Attention maps by 2 radiologists regarding the Ternary classification.

		Grades				
	Lung	0	1	2	3	4
Expert 1	Left	2	0	14	11	0
	Right	1	0	5	17	4
Expert 2	Left	2	0	15	10	0
	Right	2	0	7	16	2
Consensus	Left	2 (7%)	0	14 (52%)	11 (41%)	0
	Right	1 (4%)	0	6 (22%)	16 (59%)	4 (15%)

Table VI. Evaluation of Attention map disagreements regarding the Binary classification.

Disagreement no.	Expert 1 grade	Expert 2 grade	Consensus grade
1 (left lung of patient 2)	2	3	2
2 (left lung of patient 16)	2	2	2
3 (left lung of patient 18)	2	3	2
4 (left lung of patient 24)	2	3	2
5 (left lung of patient 27)	3	2	2
6 (right lung of patient 4)	4	3	3

Table VII. Evaluation of Attention map disagreements regarding the Ternary classification.

Disagreement no.	Expert 1 grade	Expert 2 grade	Consensus grade
1 (left lung of patient 6)	3	2	3
2 (right lung of patient 7)	3	2	3
3 (right lung of patient 14)	3	2	2
4 (right lung of patient 27)	4	0	4

binary classification, to be grades 2 and 3, indicating yet again the need for further training. The model misclassified the COVID-19 patients 8 and 15 as 'pneumonia'. The experts graded the attention map as 3 and 4 for the left and right lung of patient 8 (Fig. 8) and 2 and 4 for patient 15 (Fig. 9), respectively.

This in our view is interesting, because although the model focuses correctly at the relevant lung regions (amongst others such as the occlusion due to the heart), it does not manage to take the proper decision and to correctly classify these two images. Also, the model misclassified the COVID-19
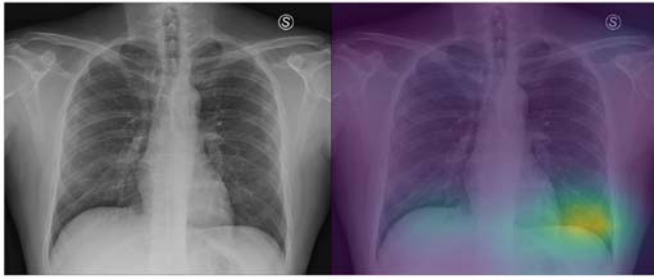
Figure 11. Attention map of patient 23 - Ternary classification - False negative COVID-19 (predicted as normal with a certainty of 98%) - Evaluated as grade 2 and 2 (left and right lungs, respectively) by the experts.

patients 10 and 23 as healthy/normal. The experts graded the attention maps as grade 2 for each lung of both patients. Given the fact that the model does not focus on the proper lung regions (as seen in Figs. 10 and 11), this misclassification can be partly attributed to this lack of focus.

Discussion

The present study focused on COVID-19 classification from routine X-ray examinations without any segmentation pre-processing step. The AI framework was evaluated in terms of quantitative metrics but also in a qualitative fashion by expert radiologists, who rated the diagnostic relevance of the attention maps of the model's convolutional part on unseen testing sets. The examined attention maps constitute an important tool in deep learning analysis, highlighting a highly probable region of deep feature extraction. Thus, according to the evaluation (criteria in Table II) by radiologists as presented in Tables IV and V, the proposed architecture mostly focuses in the lung region despite the presence of high intensity extrapulmonary areas across the X-ray images. In both binary and ternary classification around half of the cases received grade equal to 2, with the remaining half receiving grades 3-4 (Tables IV and V). No outliers (grade 0 or 1) were found in pneumonia versus COVID but three zero-graded cases were identified in ternary classification, a result that was rather expected due to the slightly lower performance achieved by those models. Despite the limited dataset in this study, the proposed framework has the potential to enhance the decision-making process by providing trustworthy predictions in terms of prediction confidence and visual cues representative of the deep learning analysis.

The results of each experiment are presented and compared to the current literature in Table III. In particular, the pre-trained Inception-v3 models achieved an AUC performance of 100% in pneumonia versus COVID-19, 96% in normal versus pneumonia versus COVID-19 and 93% for quaternary classification. It is worth mentioning that the transfer learning technique provided a strong baseline for the examined lesion, in addition to data augmentation mitigating the limited set of COVID-19 X-rays. The proposed fine-tuning scheme achieved better model adaptation for the neural and classification layers reaching state-of-the-art performance in binary classification (pneumonia versus COVID-19). Despite these encouraging results, efforts should be put into building a much larger public database of COVID-19 X-ray images, on which the research community will train and evaluate the performance of their proposed models.

Following this study, an extensive examination of modelling other imaging modalities will be explored, particularly deep learning analysis on available datasets with selected tomographic data (23) and on open databases with no data curation (https://radiopaedia.org/). For instance, He *et al* (24) developed a CT decision support system with attention map interpretation. The results of the study are similar to ours, at least in terms of classification performance (AUC 94%) but in their Grad-CAM attention maps a qualitative discrepancy was observed as the majority of the presented maps include regions (other high contrast tissue) outside the lung parenchyma. This issue is probably due to the lack of lung segmentation or detection prior to training leading the model to learn redundant information unrelated to the lung and COVID-19 infected area. These current limitations call for more advanced and interpretable deep learning and preprocessing techniques applied in large datasets in order to provide AI empowered clinical tools that can significantly contribute in the fight against COVID-19.

Availability of data and materials

Not applicable.

Authors' contributions

NT, ET and KM conceived and designed the study. NT, ET and KM researched the literature, performed analysis and interpretation of data and drafted the manuscript. EEV and AHK developed the attention map grading system and performed the evaluation of the attention maps. JSG and RLG collected and provided us with the private COVID-19 dataset. EEV, GZP, AHK, NP, DAS and AT critically revised the article for important intellectual content, and assisted in the literature search for this article. All authors agree to be accountable for all aspects of the work in ensuring that questions related to the accuracy or integrity of any part of the work are appropriately investigated, and finally approved the version of the manuscript to be published.

Ethics approval and consent to participate

Not applicable.

Patient consent for publication

Not applicable.

Competing interests

DAS is the Editor-in-Chief for the journal, but had no personal involvement in the reviewing process, or any influence in terms of adjudicating on the final decision, for this article. All the other authors declare that they have no competing interests.

References

1. Chen N, Zhou M, Dong X, Qu J, Gong F, Han Y, Qiu Y, Wang J, Liu Y, Wei Y, *et al*: Epidemiological and clinical characteristics of 99 cases of 2019 novel coronavirus pneumonia in Wuhan, China: A descriptive study. Lancet 395: 507-513, 2020.

2. World Health Organization (WHO): Report of the WHO-China joint mission on coronavirus disease 2019 (COVID-19). WHO, Geneva, 2020. https://www.who.int/docs/default-source/coronaviruse/who-china-joint-mission-on-covid-19-final-report.pdf. Accessed February 28, 2020

3. Petrakis D, Margină D, Tsarouhas K, Tekos F, Stan M, Nikitovic D, Kouretas D, Spandidos DA and Tsatsakis A: Obesity a risk factor for increased COVID 19 prevalence, severity and lethality (Review). Mol Med Rep 22: 9-19, 2020.

4. Docea AO, Tsatsakis A, Albulescu D, Cristea O, Zlatian O, Vinceti M, Moschos SA, Tsoukalas D, Goumenou M, Drakoulis N, *et al*: A new threat from an old enemy: Re-emergence of coronavirus (Review). Int J Mol Med 45: 1631-1643, 2020.

5. Farsalinos K, Niaura R, Le Houezec J, Barbouni A, Tsatsakis A, Kouretas D, Vantarakis A and Poulas K: Editorial: Nicotine and SARS-CoV-2: COVID-19 may be a disease of the nicotinic cholinergic system. Toxicol Rep: Apr 30, 2020 (Epub ahead of print).

6. Calina D, Docea AO, Petrakis D, Egorov AM, Ishmukhametov AA, Gabibov AG, Shtilman MI, Kostoff R, Carvalho F, Vinceti M, *et al*: Towards effective COVID 19 vaccines: Updates, perspectives and challenges (Review). Int J Mol Med 46: 3-16, 2020.

7. Skalny AV, Rink L, Ajsuvakova OP, Aschner M, Gritsenko VA, Alekseenko SI, Svistunov AA, Petrakis D, Spandidos DA, Aaseth J, *et al*: Zinc and respiratory tract infections: Perspectives for COVID-19 (Review). Int J Mol Med 46: 17-26, 2020.

8. Wong HYF, Lam HYS, Fong AH, Leung ST, Chin TW, Lo CSY, Lui MM, Lee JCY, Chiu KW, Chung T, *et al*: Frequency and distribution of chest radiographic findings in COVID-19 positive patients. Radiology 27: 201160, 2019.

9. Huang C, Wang Y, Li X, Ren L, Zhao J, Hu Y, Zhang L, Fan G, Xu J, Gu X, *et al*: Clinical features of patients infected with 2019 novel coronavirus in Wuhan, China. Lancet 395: 497-506, 2020.

10. Kong W and Agarwal PP: Chest imaging appearance of COVID-19 infection. Radiol Cardiothorac Imaging 2: e200028, 2020.

11. Bandirali M, Sconfienza LM, Serra R, Brembilla R, Albano D, Ernesto PF and Messina C: Chest radiograph findings in asymptomatic and minimally symptomatic quarantined patients in Codogno, Italy during COVID-19 pandemic. Radiology 295: E7, 2020.

12. Ai T, Yang Z, Hou H, Zhan C, Chen C, Lv W, Tao Q, Sun Z and Xia L: Correlation of chest CT and RT-PCR testing in coronavirus disease 2019 (COVID-19) in China: A Report of 1014 cases. Radiology: Feb 26, 2020 (Epub ahead of print).

13. Hao K: Doctors are using AI to triage covid-19 patients. The tools may be here to stay. MIT Technology Review, 2020. https://www.technologyreview.com/2020/04/23/1000410/ai-triage-covid-19-patients-health-care/. Accessed April 23, 2020.

14. Zhang J, Xie Y, Li Y, Shen C and Xia Y: COVID-19 Screening on chest X-ray images using deep learning based anomaly detection. arXiv: 2003.12338.

15. Narin A, Kaya C and Pamuk Z: Automatic detection of coronavirus disease (COVID-19) using X-ray images and deep convolutional neural networks. arXiv: 2003.10849.

16. Wang L and Wong A: COVID-Net: A tailored deep convolutional neural network design for detection of COVID-19 cases from chest X-ray images. arXiv: 2003.09871.

17. Afshar P, Heidarian S, Naderkhani F, Oikonomou A, Plataniotis KN and Mohammadi A: COVID-CAPS: A capsule network-based framework for identification of COVID-19 cases from X-ray images. arXiv: 2004.02696.

18. Abbas A, Abdelsamea MM and Gaber MM: Classification of COVID-19 in chest X-ray images using DeTraC deep convolutional neural network. arXiv: 2003.13815.

19. Khalifa NEM, Taha MHN, Hassanien AE and Elghamrawy S: Detection of coronavirus (COVID-19) associated pneumonia based on generative adversarial networks and a fine-tuned deep transfer learning model using chest X-ray dataset. arXiv: 2004.01184.

20. Ghoshal B and Tucker A: Estimating uncertainty and interpretability in deep learning for coronavirus (COVID-19) detection. arXiv: 2003.10769.

21. Ucar F and Korkmaz D: COVIDiagnosis-Net: Deep Bayes-SqueezeNet based diagnosis of the coronavirus disease 2019 (COVID-19) from X-ray images. Med Hypotheses 140: 109761, 2020.

22. Apostolopoulos ID and Mpesiana TA: Covid-19: automatic detection from X-ray images utilizing transfer learning with convolutional neural networks. Phys Eng Sci Med: https://doi.org/10.1007/s13246-020-00865-4.

23. Loey M, Smarandache F and M. Khalifa NE: Within the lack of chest COVID-19 X-ray dataset: A novel detection model based on GAN and deep transfer learning. Symmetry (Basel) 12: 651, 2020.

24. He X, Yang X, Zhang S, Zhao J, Zhang Y, Xing E and Xie P: Sample-efficient deep learning for COVID-19 diagnosis based on CT scans. medRxiv: doi: https://doi.org/10.1101/2020.04.13.20063941.

25. Zhao J, Zhang Y, He X and Xie P: COVID-CT-dataset: A CT scan dataset about COVID-19. arXiv: 2003.13865.

26. Wang S, Kang B, Ma J, Zeng X, Xiao M, Guo J, Cai M, Yang J, Li Y, Meng X and Xu B: A deep learning algorithm using CT images to screen for corona virus disease (COVID-19). medRxiv: doi: https://doi.org/10.1101/2020.02.14.20023028.

27. Bai HX, Wang R, Xiong Z, Hsieh B, Chang K, Halsey K, Tran TML, Choi JW, Wang DC, Shi LB, *et al*: AI augmentation of radiologist performance in distinguishing COVID-19 from pneumonia of other etiology on chest CT. Radiology (In Press).

28. Cohen JP, Morrison P and Dao L: COVID-19 image data collection. arXiv: 2003.11597.

29. Jeffrey RB Jr, Manaster BJ, Osborn AG, Rosado-de-Christenson ML and Woodward PJ: Diagnostic Imaging: Emergency. 2nd edition. Lippincott Williams & Wilkins, 2013.

30. Kermany DS, Goldbaum M, Cai W, Valentim CCS, Liang H, Baxter SL, McKeown A, Yang G, Wu X, Yan F, *et al*: Identifying medical diagnoses and treatable diseases by image-based deep learning. Cell 172: 1122-1131.e9, 2018.

31. Mooney P: Chest X-ray images (Pneumonia). https://www.kaggle.com/paultimothymooney/chest-xray-pneumonia. Accessed March 24, 2018.

32. Szegedy C, Vanhoucke V, Ioffe S, Shlens J and Wojna Z: Rethinking the Inception Architecture for Computer Vision. In: Proceedings of the IEEE Computer Society Conference on Computer Vision and Pattern Recognition. IEEE Computer Society, pp2818-2826, 2016.

33. Deng J, Dong W, Socher R, Li LJ, Li K and Li FF: ImageNet: A Large-Scale Hierarchical Image Database. In: Proceedings of 2009 IEEE Conference on Computer Vision and Pattern Recognition, Miami, FL, pp248-255, 2009.

34. Abràmoff MD, Lou Y, Erginay A, Clarida W, Amelon R, Folk JC and Niemeijer M: Improved automated detection of diabetic retinopathy on a publicly available dataset through integration of deep learning. Invest Ophthalmol Vis Sci 57: 5200-5206, 2016.

35. Selvaraju RR, Cogswell M, Das A, Vedantam R, Parikh D and Batra D: Grad-CAM: Visual Explanations from Deep Networks via Gradient-Based Localization. In: Proceedings of the IEEE International Conference on Computer Vision. Institute of Electrical and Electronics Engineers Inc., pp618-626, 2017.

36. Kingma DP and Ba J: Adam: A method for stochastic optimization. arXiv: 1412.6980.

37. Chowdhury MEH, Rahman T, Khandakar A, Mazhar R, Kadir MA, Mahbub Z Bin, Islam KR, Khan MS, Iqbal A, Al-Emadi N and Reaz MBI: Can AI help in screening Viral and COVID-19 pneumonia? arXiv: 2003.13145.